



Cardiac Support for the Right Ventricle: Effects of Timing on Hemodynamics-Biomechanics Tradeoff

Ileana Pirozzi¹(✉) , Ali Kight¹ , Edgar Aranda-Michael³ , Rohan Shad⁴, Yuanjia Zhu^{1,4}, Lewis K. Waldman⁵, William Hiesinger⁴, and Mark Cutkosky²

¹ Department of Bioengineering, Stanford University,
Stanford, CA 94305, USA
ipirozzi@stanford.edu

² Department of Mechanical Engineering, Stanford University,
Stanford, CA 94305, USA

³ Department of Biomedical Engineering, Carnegie Mellon University, Pittsburgh,
PA 15289, USA

⁴ Department of Cardiothoracic Surgery, Stanford University, Stanford,
CA 94305, USA

⁵ Insilicomed, La Jolla, CA, USA

Abstract. A well-established treatment option for advanced heart failure is the implantation of a ventricular assist device (VAD) in the left heart. In over one quarter of patients, however, failure of the right ventricle (RV) occurs shortly after implantation, with a paucity of options for RV failure management in this clinical context. A possible treatment for RV failure is the application of regional mechanical support to the free surface of the RV. Here, we investigate the effect of this treatment using a multiscale finite element model. We discuss a trade-off between hemodynamic benefits and biomechanical effects of simulated interventions with respect to the complex dynamics of RV contraction. Specifically, we report on timing of support with respect to the cardiac cycle, duration of applied force, and force profile distribution. Insights from these preliminary studies can be informative in the rational design of RV-specific mechanical support solutions.

Keywords: Right heart failure · Biomechanical cardiac modeling · Medical device design

1 Introduction

For decades, the focus of heart failure treatment and interventions has largely been the left ventricle, with one of the most groundbreaking technologies added to the toolkit of heart failure being the Left Ventricular Assist Device (LVAD).

I. Pirozzi and A. Kight—Equally contributing authors.

© Springer Nature Switzerland AG 2021
D. B. Ennis et al. (Eds.): FIMH 2021, LNCS 12738, pp. 385–395, 2021.
https://doi.org/10.1007/978-3-030-78710-3_37

Yet, while LVADs have provided a glimmer of hope for patients with late-stage heart failure, right heart failure (RHF) following implantation remains a highly unpredictable, often fatal complication [1,2]. To date, up to 30–40% of LVAD patients develop RHF shortly after implantation, facing a paucity of clinical management options [1,3]. Following LVAD insertion, the RV is challenged in a number of ways. First, with near normalization of cardiac output, preload increases dramatically. Second, the LVAD causes unloading of the left ventricular cavity resulting in an interventricular septal shift and altered right ventricular (RV) geometry. Third, increases in pulmonary vascular resistance and pulmonary pressures encountered in the perioperative period further compromise the failing ventricle [4]. Such complications result in RV dysfunction. With an increasing number of patients undergoing LVAD implantation, the need for easily-deployed, safe, and effective devices for temporary support of the RV will continue to grow [5]. In order to design such therapies, the mechanisms of physiological (and pathophysiological) RV dynamics must be elucidated. External, non-blood contacting solutions provide several advantages [6]. Importantly, pulsatile flow augmentation (or assistance in pump function) can be achieved across the native cardiac vasculature, without the need to divert blood through artificial circuits, and thus not incurring the risk of thrombolytic events. To promote the development of alternative, external solutions supporting the RV free wall, we propose to characterize the effects of distributed compressive forces applied on the RV, with an eye on device-tissue interactions and effects on tissue strains and deformations. These considerations are generally difficult to evaluate due to the complex, multiscale nature of cardiac physiology. Additionally, the right ventricle presents more peculiar geometry and contraction patterns than the left ventricle, incurring additional complications. To meet these challenges, we employ a widely characterized multiscale finite element analysis software package (Continuity Pro, Insilicomed, La Jolla, CA) developed specifically for dynamic cardiac modeling and extensively used for medical device modeling. Using similar methods, recent interest in direct cardiac compression (DCC) has led to preliminary investigations to evaluate the effects of external forces on the cardiac surface to aid left ventricular (LV) performance [7]. Here, we highlight the need for investigations focused specifically on the right ventricle. Despite the existence of several other etiologies of RV failure, the clinical context of LVAD implantation provides an ideal scenario for such investigations, given that LV pump function is replaced by the LVAD. Specifically, any external device would provide a finite amount of energy to be applied to the ventricular surface. The goal of this study is to identify physically-interpretable conditions to apply such finite energy to maximise cardiac output and performance. To achieve long-term sustainable outcomes and promote myocardial health, ventricular deformations resulting from the application of such forces must also be minimized, in order to prevent the onset of adverse cardiac remodeling and ensure viability of this approach [8]. Such insights will aid the development of engineered solutions tailored to the RV complex shape, motion profiles, and function.

2 Methods

Stable beating-heart simulations were established using a multiscale finite element analysis software package for dynamic cardiac modeling (Continuity Pro, Insilicomed, La Jolla, CA) [7,9]. Continuity Pro (CPro) recapitulates patient-specific cardiac mechanics and electrophysiology by combining imaging-derived cardiac geometry and 3D fiber architecture, a dynamic model of calcium excitation-contraction coupling dynamics, and a lumped parameter circulatory model to simulate the function of the beating heart through both systemic and pulmonic vasculature. A transversely isotropic constitutive law, adapted from previous work was employed alongside a Fung-type hyperelastic model with exponential strain energy density function [10]. Interested readers can find in-depth description of the software and the patient-based model employed in these experiments in previous work [11].

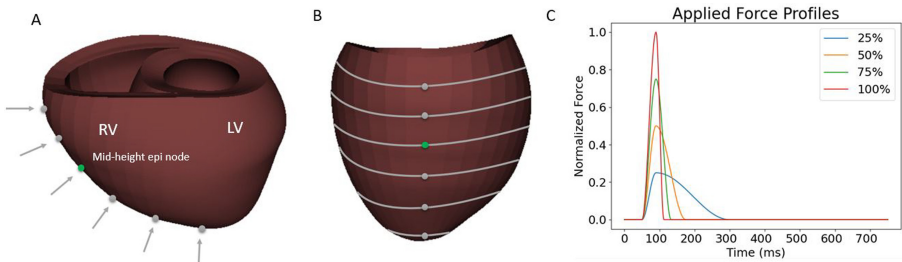


Fig. 1. Experimental model setup. A) Rendering of human biventricular model with applied nodal compressive forces. The mid-height endocardial node used for biomechanical analysis is shown in green. B) Rendering of the biventricular model displaying RV free wall. C) Time-varying force profiles of 25%, 50%, 75%, and 100% max force, over one cardiac cycle (Color figure online)

The human biventricular model employed in the following analyses is shown in Fig. 1. The model consists of 192 tri-cubic Hermite elements and 282 nodes, a refinement determined in previous work to obtain sufficient longitudinal resolution with respect to biomechanical metrics of interest [7]. The resulting refinement provides 6 longitudinal nodes at which compressive forces are applied during contraction (defined as $0 < t < 300$ ms, over a cycle duration of 750 ms). Specifically, the coordinate system for the strain tensor was selected as the orthonormal basis of the local fiber coordinate system, with each fiber having (1) a direction along its own axis, (2) a direction perpendicular to the fiber and along the surface of the heart, and (3) a direction perpendicular to the fiber and directed radially towards the lumen. E11, E22 and E33 are thus the normal strains in the fiber, cross-fiber and radial directions respectively. The first principal strain is denoted as P3. Details and illustrations on the selected coordinate system are described in extensive detail in previous work [12].

In this study, CPro was used to generate beating-heart simulations of a patient-specific model with anatomic dimensions congruent with a severe case of dilated cardiomyopathy and a LV ejection fraction of 16%, consistent with a clinical scenario benefiting from LVAD support. To simulate the effect of an external support device, compressive forces were applied to the LV and RV free wall epicardial surfaces using force boundary conditions established as a function of time throughout the cardiac cycle. Simulations were run at constant heart rate of 80 beats per minute and aortic valve opening defined as the end of isovolumetric contraction, IVC ($t = 146$ ms, where $t = 0$ is end-diastole).

A total of five beating-heart simulations were set up (see Fig. 1B): one baseline case where no external support is applied and four applied-force cases. The four active force simulations were prescribed time-varying force profiles applied to epicardial nodes and normal to the RV free wall surface throughout contraction. The maximum applied force to the epicardial RV is 0.4 N while the LV was kept at a constant 1 N throughout the simulations. The maximum force magnitude was informed by previous experimental work optimizing RV epicardial restraint pressure, with the goal of optimally reducing end-diastolic wall stress without impairing filling [13]. The integral of the force-time graph was kept constant at 31.25 N.s across all simulations in order to simulate a finite amount of energy available from a prospective device, and to investigate the effect of timing of the applied force on cardiac dynamics. To simulate the use of a device applied to the entire epicardial surface, 6 points along the longitude of the RV free wall were selected for force application (Fig. 1A). Force profiles were chosen based on reasonable expectations of physically realizable devices that could achieve similar force-time behavior. Peak forces were selected to be within physiological ranges. Particular consideration was given to the fact that higher RV peak pressure may result detrimental to pulmonary remodeling and have deleterious effects on pulmonary vasculature. Throughout the report, the four applied-force cases are referenced as a percentage of the maximum force case on the RV side: cases 25–100, corresponding to 25–100% of max force respectively. Time-varying force profiles for each simulated case are shown in Fig. 1C.

It is worth noting that, as this is an LV failure model, moderate compression was also applied to the LV and kept constant throughout the parametric simulations. The relevance of this simulated input to the physical case of LVAD support is discussed in later sections.

3 Results

Hemodynamic Analysis. The hemodynamic variables presented are end-systolic volume (ESV), end-diastolic volume (EDV), stroke volume (SV, defined as the difference between EDV and ESV), stroke work (SW, defined as the product of pressure and volume) and ejection fraction (EF, defined as SV/EDV). All RV hemodynamic metrics are reported in Fig. 2 as a percentage improvement of each applied-force case (25%, 50%, 75% and 100%) from the baseline case. The five aforementioned metrics were selected for their established relevance to cardiac performance. In patients with dilated cardiomyopathy, increases in EDV can

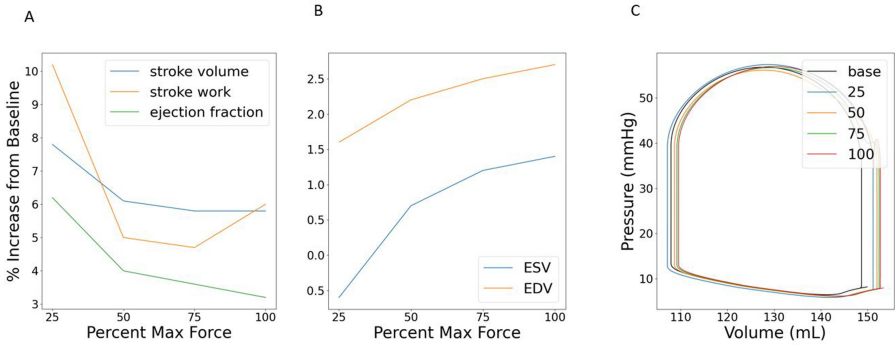


Fig. 2. Right ventricular (RV) hemodynamic variables as a function of percent max force. A) Stroke volume and stroke work, B) EDV and ESV. On average, hemodynamic benefit decreases as the percent max force increases. Note: Hemodynamic benefit is defined as minimized EDV and ESV, and maximized stroke work and stroke volume. C) Pressure-Volume loops for all cases

induce adverse tissue strains triggering a long-term process of ventricular remodeling and should thus be minimized [8]. Similarly, increases in ESV, for a given EDV, demonstrate decreased contractile function and are thus also undesirable [14]. SV, SW and EF on the other hand, are measures of cardiac output in each contraction, and increases are considered hemodynamically beneficial. Based on these insights, we note a clear trend of diminishing hemodynamic benefit across all hemodynamic parameters with increasing peak force. One interesting exception to this trend can be seen in Fig. 2A, where stroke work improvement does not monotonically decrease from 25 to 100% max force, but rather reaches a nadir at 75%. The trend is more pronounced in SW than SV due to the compounded contribution of both volume and pressure to the calculation of SW. Stroke volume is a particularly interesting metric as it is directly related to cardiac output, assuming constant heart rate. The aforementioned metrics can also be visualized through pressure-volume loops, illustrated in 2C for baseline and each applied-force case, While the primary focus of this study is on the RV, the authors also report improvements in EF in the LV, which is a critical measure of systolic function. The greatest improvement of left ventricular EF was 7.84%, corresponding to the 25% force case.

Biomechanical Analysis. Biomechanical analysis is performed on selected nodes at mid-ventricular height on the RV free wall surface, as this region undergoes substantial deformation during the cardiac cycle [15]. The model offers sufficient radial refinement to analyze transmural trends in mechanical behavior. Specifically we select three mid-height nodes for analysis: one epicardial, one in the midwall and one epicardial (see Fig. 3B inset). In Fig. 3 we report aggregate transmural trends in strain deviation from the baseline case (i.e. no external support applied). The maximum increase in strain is reported for each applied force case with respect to each of the three transmural nodes. We observe an inverse

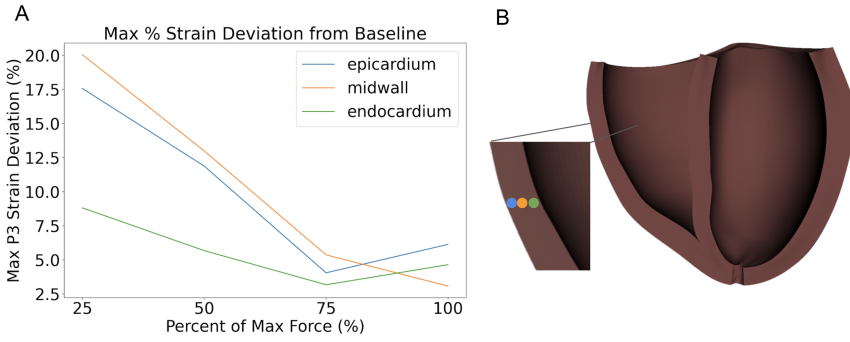


Fig. 3. Max Percent Strain Deviation from baseline case. A) deviation of principal strain between applied force trials and baselines case for transmural mid-height nodes; B) cross-sectional view of biventricular model; inset: location of epicardial (blue), mid-wall (orange) and endocardial nodes (green). Note: Strain deviation from baseline (healthy RV case) should be minimized (Color figure online)

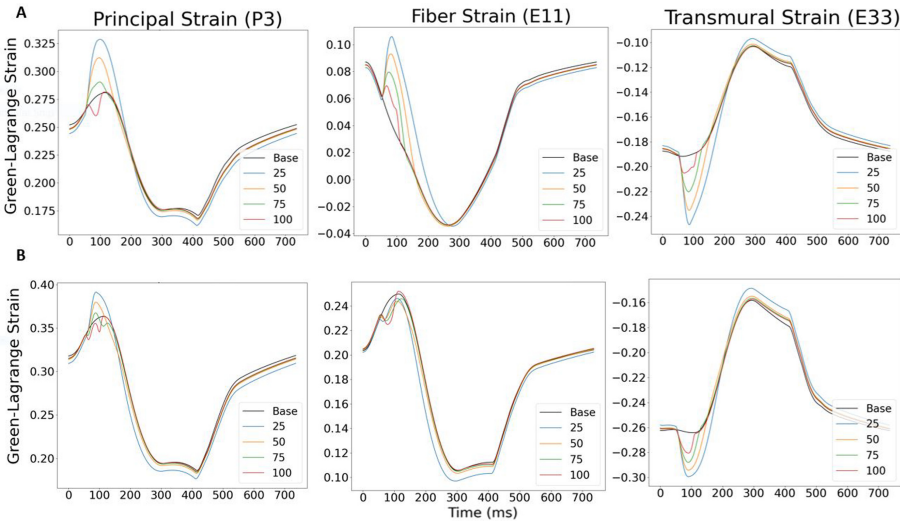


Fig. 4. Time-series analysis of Green-Lagrange Strain (P3, E11, E33) at mid-height nodes for one cardiac cycle where $t = 0 \text{ ms} = \text{end diastole}$; $t = 146 \text{ ms} = \text{aortic valve opening}$. BL = Baseline case. A) epicardial mid-height node, B) endocardial mid-height node

relationship between the applied load and the maximum principal strain, with a local minimum occurring at the 75% force case (Fig. 3). The midwall element experiences the greatest increase in strain (up to 20% from baseline), followed closely by the epicardial node, on which the force is applied. The endocardial node experiences the least increase in strain (max at 8% in the 25 case). Time-series data for the epicardial and endocardial mid-height nodes is presented in

Fig. 4. The first column of panels displays time-series data of the first principal strain (P3). The second and third columns display principal strain decomposition into fiber-directed components (E11) and transmurally-directed components (E33). The transmural strain (E33) is compressive, indicating a larger cavity volume, and becomes less compressive with the increasing RV load, accounting for the sharp increase in strain from baseline. Fiber strain (E11) exhibits a sharp increase peaking shortly around 150 ms, which coincides with the administration of the external force. Due to the incompressibility of cardiac tissue, the compressive strain in the transmural direction results in an tensile strain in the fiber direction.

We note that in the endocardium, P3 strain shows a much more pronounced E11 implication than the epicardium. This difference is likely due to the transmurally variable direction of cardiac fibers, as discussed in a later section. Moreover, the transmural strain (E33) is compressive, indicating a larger cavity volume, and becomes less compressive with the increasing RV load. Finally, the effects of the RV geometry are seen as the fiber strain (E11) plays little role in the endocardial node, a finding that differs from prior work examining the LV under compression [7]. This is likely attributable to the crescent, asymmetric shape of the RV compared to the prolate shape of the LV.

Maximum deviations in P3 strain for each experimental case, occurring during mid-isovolumetric contraction (around 100 ms), are also graphically represented in Fig. 5 for the RV free wall view and the cross-sectional biventricular views. The observed trend extends transmurally throughout the RV free wall midsection and beyond the mid-height node used for analysis. The cross-sectional view (Fig. 5B) demonstrates two trends: (1) the RV geometrical conformation shifts from more enlarged at 25% force case, to more compressed at the 100% case, assuming a typical crescent-shape conformation; (2) the transmural strain concentration across the RV wall decreases as RV force is increased.

4 Discussion

The development of technologies for heart failure have been historically focused on the left ventricle. Mechanical interventions for left heart failure have benefited from ample research and development, whereas tailored support for the right heart remains lacking in comparison. Previous computational studies have investigated ideal epicardial pressure for direct cardiac compression devices, demonstrating that ventricle-specific requirements differ substantially between the left and right ventricles [9]. To our knowledge, we present the first study set out to quantitatively investigate the effect of externally applied forces in aiding ventricular contraction and describe the interplay between hemodynamic and biomechanical effects in the RV. In the context of a post-LVAD implantation RV failure, it is critical for RV mechanical support interventions to enhance hemodynamic function and ensure a comparable cardiac output to the supported LV. In this study, the physical rationale behind the experimental design was to test the effects of a prospective external device exerting a finite amount of energy on the

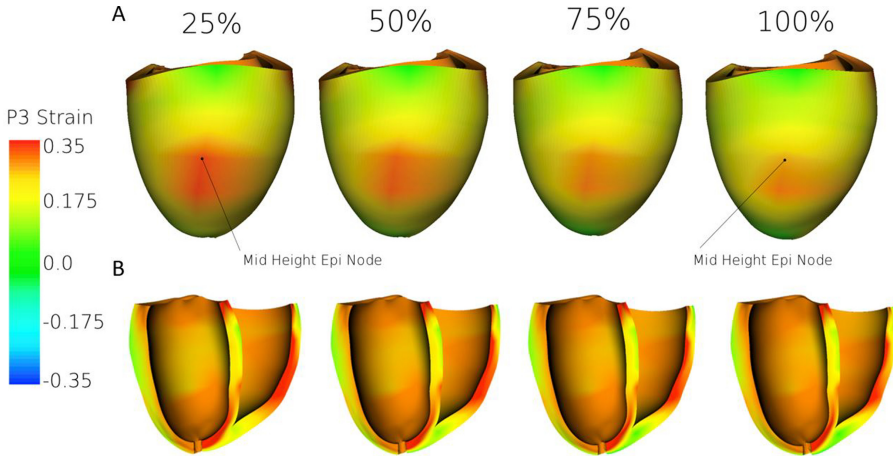


Fig. 5. Principal Strain Maps during Isovolumic Contraction (IVC) - A) RV Free Wall View. Maximum principal strain is plotted for each applied force case, 25%, 50%, 75% and 100%. Strain concentrations in the mid-ventricular free wall display a decreasing trend. B) Cross-sectional Biventricular View. Maximum principal strain is plotted for each applied force case, 25%, 50%, 75% and 100%.

RV free wall surface. Against the authors' initial intuition, lower peak applied force results in a larger stroke work than higher peak forces (10% increase from baseline compared to 5%, 4.5% and 6% for the four cases respectively), suggesting that force duration could be a more powerful predictor of hemodynamic benefit compared to peak magnitude.

Alterations to the complex biomechanics of myocardial tissue have been implicated as contributing factors to adverse ventricular remodeling, a mechanism universally proposed to underpin the pathophysiology of heart failure [16,17]. Therefore, it is imperative for interventions to be designed to minimize alterations to baseline regional biomechanics. Results of comparative biomechanical analysis of the four models tested demonstrate that the maximum strain deviation from baseline decreases as percent max force increases. This trend opposes the aforementioned hemodynamic observations, in that beneficial effects occur at higher percent max force and shorter force duration. Together, the contrasting effects imply a trade-off between hemodynamic benefit and biomechanical alterations with respect to force magnitude and timing. Increasing the duration of the applied force with lower magnitude seems to positively affect pump function but has a negative effect on tissue biomechanics. Surprisingly, deviation from baseline appears larger in the midwall as compared to the epicardial wall; an observation that can be attributed to the geometry of the RV and the myocardial fiber angle. In the midwall, the fibers are circumferentially aligned, meaning that the fiber strain, which is a major component of the principal strain, is closely related to hoop stress at this depth in the myocardium.

When force is applied, the hoop stress, and associated strain, decreases substantially.

One important observation is the seemingly incongruous finding that increasing force on the RV both increases the end diastolic volume (Fig. 2B) while also decreasing the maximum principal and fiber strain (Fig. 4). First, it may be counterintuitive that the application of epicardial forces results in increased volume parameters (ESV, EDV - see Fig. 2). However, it must be noted that this simulation provides transient support during contraction (not expansion), and the adaptive circulatory model in the ContinuityPro software responds by increasing systemic flow-back and thus increasing preload. Additionally, upon first inspection, it may seem logical that increasing EDV would cause an increased distention in the RV myocardium, resulting in increased strain. However, RV geometry plays a crucial, yet subtle, role. While the LV generally embodies a prolate shape with an axis-symmetric behavior, the RV presents and much more complex shape [18, 19]. A possible interpretation is that, while the EDV is increasing as a whole in the RV, expansion is not uniform throughout the crescent shaped cavity, with some regions distending more than others (see Fig. 5). Upon inspection of different nodes in the model, such intuitions are confirmed by the evident disparity in regional deformations. Such findings are consistent with experimental studies attempting to characterize the RV's irregular motion, which previously concluded that the RV displays a clear pattern of regionally varying mechanical activation [20]. Specifically, the mid-height epicardial section where force is applied undergoes a decreased deformation with increasing force. While this specific finding is interesting in its own right, it also points to the more generalizable observation that these computational methods are necessary to address such discrepancies, especially ones which are intimately involved with patient specific geometry.

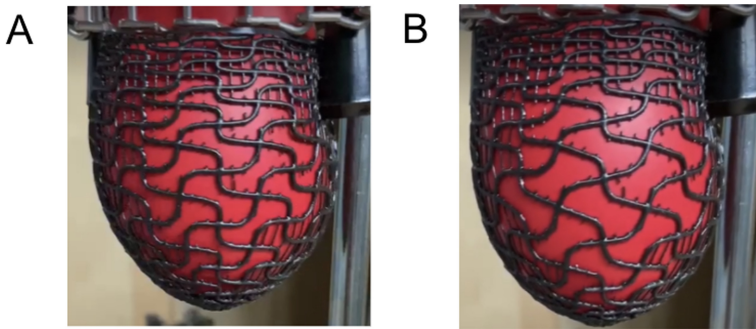


Fig. 6. Prototype of elastic metamaterial sleeve. A) Systolic conformation, B) Diastolic conformation

5 Conclusion and Implications for Device Design

In this study, we investigated the effects of external mechanical support on the RV to elucidate physically interpretable insights to inform the design of prospective devices. Studies leveraging modeling approaches have previously demonstrated that the interplay between hemodynamic and biomechanical effects of interventions can be surprising and counter-intuitive. For example, studies aimed at evaluating the effects of isotropic stiffening of newly infarcted cardiac tissue found no net hemodynamic benefit despite substantial alteration in mechanical properties - an effect that was later validated experimentally in a large animal model [21]. Similarly, it is worth noting that the results of the present study also contrast the authors' original predictions. It was initially hypothesized that a lower magnitude force delivered over a longer time period (i.e. the 25% case), would be biomechanically favorable and hemodynamically unfavorable compared to a higher, impulse-like force, the 100% case. Instead, the results show the opposite trend, evidencing the complex dynamics of cardiac function.

Nevertheless, these findings are useful to inform the design of physically realizable mechanical systems based on favorable force profiles characterized in this report. For example, elastic structures can be designed and tuned to display desired energy release dynamics, by modifying properties such as effective stiffness. Mechanical design coupled with additive manufacturing can be leveraged to yield smart mechanical metamaterials with effective stiffness properties that change as a function of time or deformation. An example of this approach is provided in Fig. 6, where early prototypes of an elastic, metamaterial support sleeve are shown. The two panels show the different configurations of the sleeve in systole (A) vs. diastole (B) in a benchtop setup. The passive support behavior was achieved using auxetic motifs, patterned onto a ventricular surface, to simulate ventricular mechanical behavior. Further investigation of material behavior and effective support provided by passive structures to ventricular tissue is warranted through %in-vitro and %in-vivo studies following initial computational findings.

Overall, we believe the elucidation and quantification of the trends exposed in this preliminary study can provide insight for the rational design of patient-specific mechanical support for LVAD-adjunct therapies aimed at supporting the right heart. Future investigations can build on this work by designing force profiles representative of physically realizable mechanical elements.

References

1. Argiriou, M., et al.: Right heart failure post left ventricular assist device implantation. *J. Thorac. Dis.* **6**(Suppl. 1), S52 (2014)
2. Lampert, B.C., Teuteberg, J.J.: Right ventricular failure after left ventricular assist devices. *J. Heart Lung Transplant.* **34**(9), 1123–1130 (2015)
3. Tang, P., et al.: Right ventricular failure following left ventricular assist device implantation is associated with a preoperative pro-inflammatory response. *J. Cardiothorac. Surg.* **14**, 80 (2019)

4. Kapur, N.K., et al.: Mechanical circulatory support devices for acute right ventricular failure. *Circulation* **136**(3), 314–326 (2017)
5. Sidney, S., Go, A.S., Jaffe, M.G., Solomon, M.D., Ambrosy, A.P., Rana, J.S.: Association between aging of the us population and heart disease mortality from 2011 to 2017. *JAMA Cardiol.* **4**(12), 1280–1286 (2019)
6. Horvath, M.A., et al.: An intracardiac soft robotic device for augmentation of blood ejection from the failing right ventricle. *Ann. Biomed. Eng.* **45**(9), 2222–2233 (2017)
7. Aranda-Michel, E., Waldman, L.K., Trumble, D.R.: Left ventricular simulation of cardiac compression: hemodynamics and regional mechanics. *PLOS ONE* **14**(10), e0224475 (2019)
8. Cokkinos, D.V., Belogiannas, C.: Left ventricular remodelling: a problem in search of solutions. *Eur. Cardiol. Rev.* **11**(1), 29 (2016)
9. Han, J., Kubala, M., Aranda-Michel, E., Trumble, D.R.: Ventricle-specific epicardial pressures as a means to optimize direct cardiac compression for circulatory support: a pilot study. *PLOS ONE* **14**(7), e0219162 (2019)
10. Guccione, J.M., McCulloch, A.D., Waldman, L.K.: Passive material properties of intact ventricular myocardium determined from a cylindrical model. *J. Biomech. Eng.* **113**(1), 42–55 (1991)
11. Kerckhoffs, R.C.P., Neal, M.L., Gu, Q., Bassingthwaighte, J.B., Omens, J.H., McCulloch, A.D.: Coupling of a 3d finite element model of cardiac ventricular mechanics to lumped systems models of the systemic and pulmonic circulation. *Ann. Biomed. Eng.* **35**(1), 1–18 (2007)
12. Costa, K.D., Hunter, P.J., Wayne, J.S., Waldman, L.K., Guccione, J.M., McCulloch, A.D.: A three-dimensional finite element method for large elastic deformations of ventricular myocardium: II-prolate spheroidal coordinates. *J. Biomech. Eng.* **118**(4), 464–472 (1996)
13. Cevasco, M., et al.: Right heart failure: an ischemic model and restraint therapy for treatment. *Ann. Thorac. Surg.* **97**(4), 1356–1363 (2014)
14. Kerkhof, P.L.M.: Characterizing heart failure in the ventricular volume domain. *Clin. Med. Insights Cardiol.* **9**, 11–31 (2015)
15. Truong, V.T., et al.: Cardiac magnetic resonance tissue tracking in right ventricle: feasibility and normal values. *Magn. Reson. Imaging* **38**, 189–195 (2017)
16. Mann, D.L., Bristow, M.R.: Mechanisms and models in heart failure: the biomechanical model and beyond. *Circulation* **111**(21), 2837–2849 (2005)
17. Kurrelmeyer, K., et al.: Cardiac remodeling as a consequence and cause of progressive heart failure. *Clin. Cardiol.* **21**(S1), 14–19 (1998)
18. Gripari, P.: Right ventricular dimensions and function: why do we need a more accurate and quantitative imaging? *J. Cardiovasc. Echography* **25**, 19–25 (2015)
19. Lang, R.M., et al.: Recommendations for cardiac chamber quantification by echocardiography in adults: an update from the American Society of Echocardiography and the European Association of Cardiovascular Imaging. *J. Am. Soc. Echocardiogr.* **28**, 1–39 (2015)
20. Auger, D.A., Zhong, X., Epstein, F.H., Spottiswoode, B.S.: Mapping right ventricular myocardial mechanics using 3d cine dense cardiovascular magnetic resonance. *J. Cardiovasc. Magn. Reson.* **14**(1), 4 (2012)
21. Fomovsky, G.M., Macadangdang, J.R., Ailawadi, G., Holmes, J.W.: Model-based design of mechanical therapies for myocardial infarction. *J. Cardiovasc. Transl. Res.* **4**(1), 82–91 (2011)